Progression Rate of Backward Erosion Piping: Small Scale Experiments

J.C. Pol[1], W. van Klaveren[2], W. Kanning[3], V.M. van Beek[4], B.A. Robbins[5], S.N. Jonkman[6]

[1]Delft University of Technology & HKV Consultants, Stevinweg 1, Delft, The Netherlands; e-mail: j.c.pol@tudelft.nl. Corresponding author.
[2]Delft University of Technology; e-mail: wouter_vanklaveren@hotmail.com
[3]Delft University of Technology & Deltares; e-mail: w.kanning@tudelft.nl
[4]Deltares; e-mail: vera.vanbeek@deltares.nl
[5]U.S. Army Corps of Engineers & Colorado School of Mines; e-mail: bryantrobbins@mymail.mines.edu
[6]Delft University of Technology; e-mail: s.n.jonkman@tudelft.nl

ABSTRACT

Most research on backward erosion piping (BEP) focuses on the critical conditions leading to failure. This paper studies the development of piping over time once the critical conditions are exceeded, which is useful to estimate time to failure. A commonly used small scale rectangular box setup is modified in order to monitor pore pressures and pipe pressures with a high spatial and temporal resolution. The experimental program includes three different sand types to study the effects of grain size and compaction, and different degrees of hydraulic loading. The results indicate that the transport of particles in the pipe affects the progression rate, and that the progression rate is related to the bed shear stress in the pipe.

INTRODUCTION

Internal erosion causes a significant percentage of dike and dam failures (Danka and Zhang 2015). For dikes, backward erosion piping is the most common form of internal erosion because of the cohesive deposits on top of sandy aquifers. Backward erosion piping occurs when seepage under a dike erodes a granular dike foundation that is covered by a cohesive roof, forming a hydraulic shortcut. If a blanket is present at the polder side, this blanket has to rupture first. Subsequently, the eroded sand is deposited around the defect as a sand boil.

Most previous research on this failure mechanism has focused on the critical head difference that ultimately leads to failure and the influence of aquifer geometry and sand properties on this critical load (e.g., Bligh 1910; Hanses 1985; Sellmeijer 1988; Van Beek 2015). Such a steady state approach, which neglects time to failure, may provide sufficient information in many cases, for example in rivers with relatively long floods. When the flood duration is short compared to the time scale of backward erosion, a dike may survive a short flood, whereas it would fail under a long flood. This phenomenon potentially increases the calculated safety level of the dike and is also important for emergency response planning.

This raises the question of how to predict the development of the backward erosion process over time. A few researchers have reported progression rates in piping experiments (Robbins et al. 2017; Vandenboer et al. 2019b; Allan 2018; Pol et al. 2019). Their results show that the progression rate is related to head difference, grain size and degree of compaction. Progression rates vary several orders of magnitude between experiments with different setups and sand types. However, there is no well-validated model in the literature to predict the development of the pipe length over time. Kézdi (1979) proposed that the progression rate is proportional to the pore flow velocity, but this relation has not been validated experimentally.

The goal of this study is to establish a larger set of experiments and to explore which model approach would be suitable to predict temporal development (i.e. progression rate). We modified a commonly used laboratory setup in order to measure pore pressures and pipe pressures during the piping process with a high spatial and temporal resolution. The experimental program includes different sand types to study the effects of grain size and compaction.

EXPERIMENTAL METHOD

Modification of box-type setup

Researchers who have investigated progression rates in backward erosion piping have either used a box-type setup (Vandenboer et al. 2019b; Allan 2018) or a cylinder-type setup (Robbins et al. 2017). An advantage of the box-type setup is that it poses less restrictions on flow from the sides. On the other hand, the cylindrical shape causes the pipe to grow along an a-priori known path. This allows one to place pressure sensors right in the pipe. To combine the advantages of both types, we modified the box-type setup used by Van Beek (2015) and Vandenboer et al. (2019b) so that pipe pressures can be measured.

The inner dimensions of the box (Figure 1) are 0.48 x 0.30 x 0.1 m. It has a 10 mm thick acrylate cover plate with a 6 mm diameter exit hole (see Figure 1). The seepage length L is 0.35 m. The modification consists of two steps. First, two permeable barriers of filter fabric (0.05 mm aperture) were placed longitudinally to prevent pipe growth to the sides but allow flow from the sides. The distance between the barriers is 35 mm. Second, silicon strips (0.3 mm high, 3 mm wide, 10 mm long) were placed diagonally and sand was sprinkled over them while the silicon dried (dark grey strips in Figure 1). These two steps restrict the pipe path to the middle 15 mm of the box, without significantly influencing the flow. Hereby, the pipe can meander slightly, while also being close enough to be detected by the sensors. Locally at the interface with the guides, there may be a slightly higher porosity as the grains do not interlock with other grains. However, this effect is expected to be small, as the pipe tip generally propagates at some distance from the guides. Finally, pressure ports were made with 20 mm spacing in the center axis of the box and connected to pressure sensors at the side of the box. This sideward placement makes it easier to inspect the pipe visually from above. Influence of the ports on progression is expected to be negligible, given their limited volume.

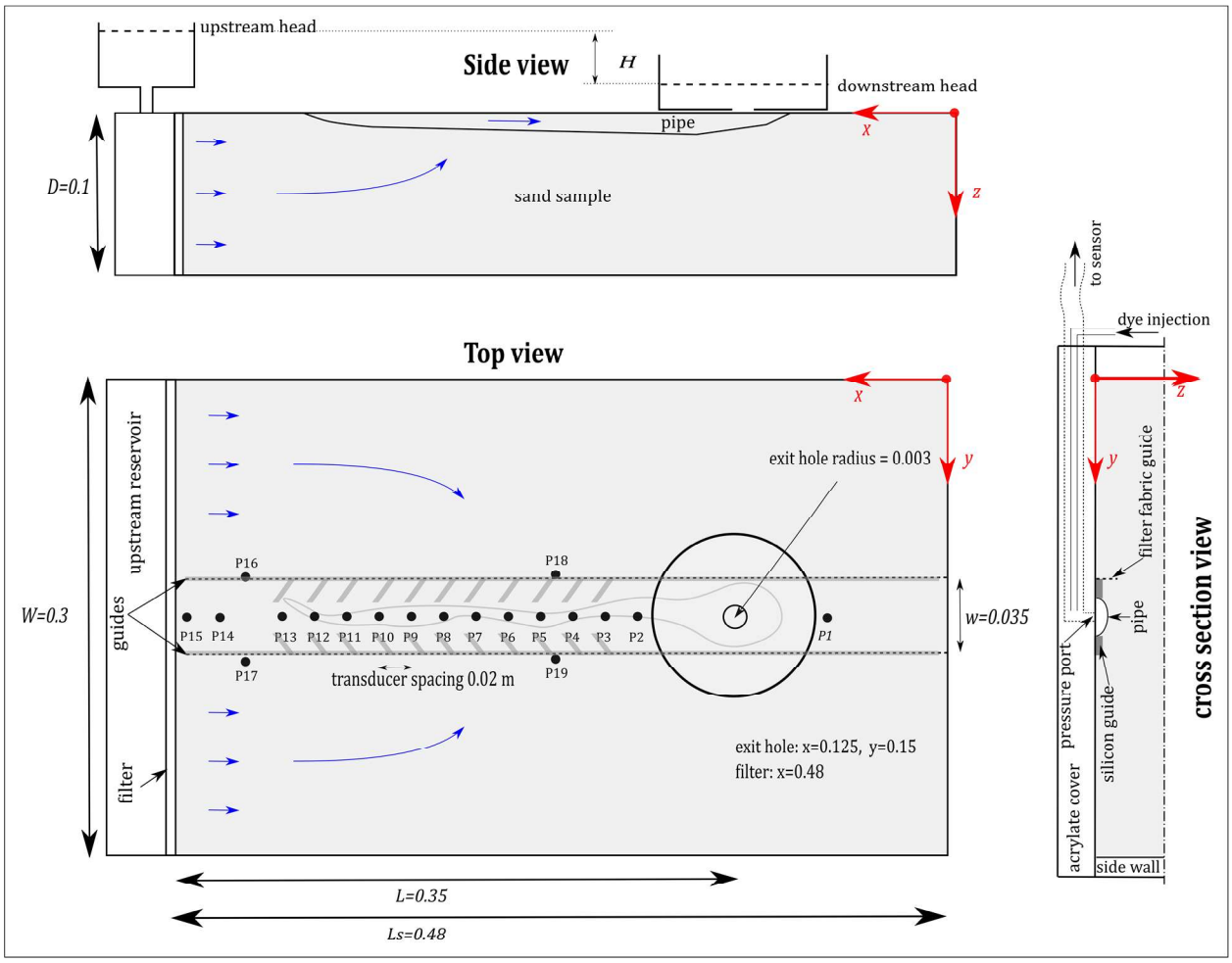

Figure 1. Experimental setup. Dimensions in meters.

Materials and Measurement Techniques

The experiments include three uniform fine to moderate fine sand types ($185<d_{50}<422$ μm). See Table 1 for an overview of characteristics.

Table 1. Sand characteristics.

Parameter	***Unit***	***FPH fine***	***Baskarp B25***	***FS35***
grain size d_{10}	mm	0.127	0.150	0.328
grain size d_{50}	mm	0.185	0.228	0.422
grain size d_{60}	mm	0.202	0.246	0.442
grain size d_{70}	mm	0.223	0.260	0.462
uniformity C_u	-	1.6	1.6	1.35
min. porosity n_{min}	-	0.361	0.352	0.344
max. porosity n_{max}	-	0.485	0.459	0.444
particle density ρ_s	kg/m^3	2610	2650	2650

The upstream and downstream water level was measured manually using riser tubes every five minutes. Pore pressure was measured by differential pressure transducers, at the locations P1-P19 shown in Figure 1, at a sampling frequency of 10 Hz. The flow rate was measured every five minutes by reading the water mass increase from a digital scale.

The erosion development was recorded by three cameras. A camera above the setup provides a top view of the sand sample, at a sampling frequency of 1/10 Hz. In some tests, we recorded short close-up videos of the erosion process using a second camera, which was placed temporarily on top of the cover. The third camera recorded the volume of the eroded sand, at a sampling frequency of 1/60 Hz. Pipe length and sand boil diameter were determined visually, although these can also be derived from the photos. The pipe depth was measured only in equilibrium conditions, using a laser device which was mounted on a movable frame to create transects perpendicular to the pipe direction.

Pipe flow velocities in equilibrium conditions were obtained by video analysis of a dye tracer. While the top camera was recording a video, a red dye was injected under low pressure through one of the pressure ports for approximately 2 seconds.

Test procedure

The test procedure consists of sample preparation, loading, and measurement cycles. First, the sand sample is prepared with the box in vertical position by sprinkling dry sand in de-aired water, and the sample is compacted by tapping the box with a hammer. Then, the box is placed in horizontal position and the head at both sides of the sample is leveled. The loading procedure is as follows: keep the head difference constant if there is still erosion after 5 minutes, or increase it otherwise. The head difference is increased by reducing the downstream head, and the upstream head is kept constant. When the pipe reaches the upstream filter, the head difference is decreased until the erosion process stops. In these equilibrium conditions, the pipe geometry and pipe flow velocity are measured.

Test program

The test program consists of two phases. Tests in phase 1 verify that the changes in experimental setup do not influence the most important results: critical head difference and average progression rate. These tests are outside the scope of this paper, but it is noted that the adapted setup gives similar results as the original one (5% lower H_c and 14% higher progression rate).

The tests in phase 2 vary in grain size, compaction and hydraulic loading (see Table 2). Densely packed samples have a relative density (*RD*) of 0.7-0.8 and the *RD* in loose samples is 0.5-0.55. Loading scenario L1 is as described in section 4.3; so gradually increase the head difference to the critical head difference (H_c) and then keep it constant. L3 and L4 are overloading scenarios, which means that after a stable pipe ($l \approx 0.10$ m) has formed, the head is increased to $1.2 \cdot H_c$ and $1.1 \cdot H_c$ respectively and then kept constant.

Table 2. Overview of experiments with adapted setup.

Test	*Sand Type*	*RD [-]*	*Load*	*k [m/s]*	*Test*	*Sand Type*	*RD [-]*	*Load*	*k [m/s]*
B25_232	B25	0.796	L1	2.70E-04	FS35_242	FS35	0.708	L3	8.70E-04
B25_233	B25	0.545	L1	3.60E-04	B25_243	B25	0.792	L1	2.60E-04
B25_234	B25	0.545	L1	3.70E-04	B25_244	B25	0.558	L1	3.30E-04
FPH_235	FPH	0.738	L1	1.10E-04	B25_245	B25	0.577	L1	3.10E-04
B25_236	B25	0.777	L1	2.50E-04	FS35_246	FS35	0.718	L1	9.00E-04
FPH_237	FPH	0.791	L1	1.10E-04	B25_247	B25	0.797	L3	2.40E-04
FS35_238	FS35	0.671	L1	1.00E-03	B25_248	B25	0.799	L3	2.50E-04
FS35_239	FS35	0.768	L1	9.00E-04	B25_249	B25	0.804	L4	2.00E-04
FS35_240	FS35	0.490	L1	1.2E-03	B25_250	B25	0.799	L4	2.50E-04
FS35_241	FS35	0.492	L1	1.20E-03					

RESULTS

General observations on the erosion process

Each test shows several phases: fluidization of sand under the exit hole, formation of a circular void around the exit hole, pipe growth towards an equilibrium (regressive) and progressive pipe growth until the pipe forms a hydraulic shortcut (see Figure 2). These phases were also observed in other experiments with the hole-type exit (e.g. Miesel 1977; Van Beek 2015; Vandenboer et al. 2019b).

The location in the pipe where grains first eroded after a head increase is not always the same. Visual observations during the head increase indicate that erosion sometimes starts in the bed, sometimes at the tip. This suggests that both the bed and the tip are close to critical conditions, at least in the regressive phase.

The erosion process at the pipe tip was studied using close-up videos. Grain detachment at the tip generally occurred in cycles. First, the porosity increased in a zone upstream of the tip, which was observed by a small displacement of particles in downstream direction. Sometimes, there was also rearrangement of a few small particles in the sand upstream of the tip. Immediately after the porosity increase, a group of grains detached and slid into the pipe. Part of the group washed away directly, while another part settled close to the tip. These settled grains were transported gradually until the cycle repeated. Between the group detachments, also individual particles detach. At higher progression rates (e.g., in the coarser FS35 sand), it was more difficult to distinguish separate cycles and the erosion process is more continuous. So, the presence and duration of all steps in the erosion cycle varies between and within tests, but the process generally followed this cycle.

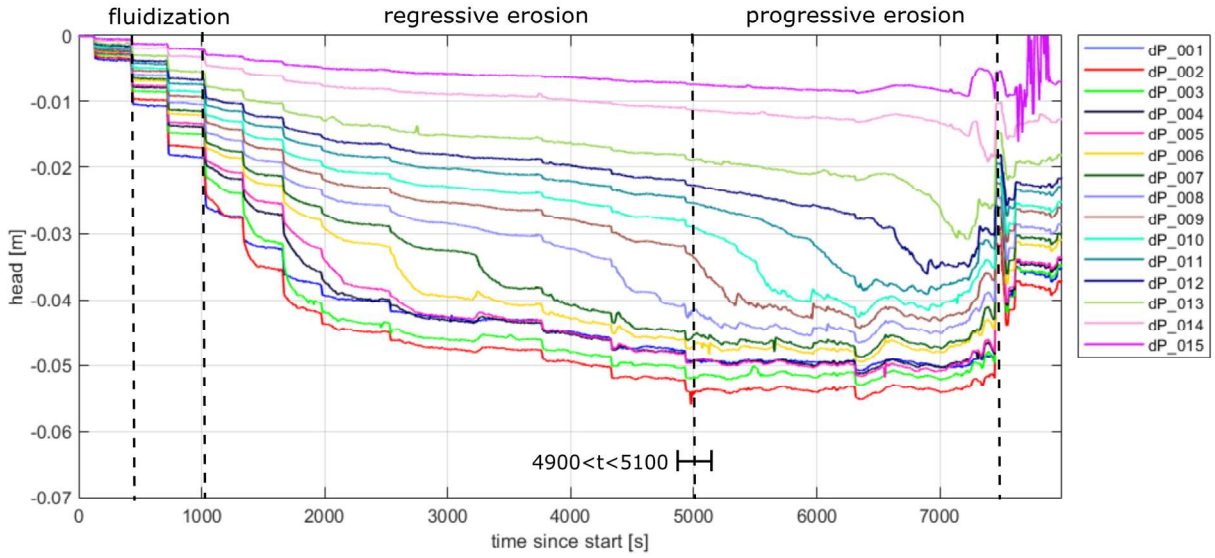

Figure 2. Head development in sensor P1-P15 and erosion phases in test B25_245. "dP" indicates sensors, located from downstream to upstream

Effect of group detachment on pressures and hydraulic gradients

One test (B25_245) includes a close-up video of the tip during a transition from equilibrium to erosion with some particle detachment in groups. In this case, the pipe tip also grows closely under the pressure sensors. At the start of the video, the tip is right under P8, and the shortest distance from the other sensors to the pipe during its development is approximately 1 mm (P2,P3,P7), 2 mm (P6) and 7 mm (P4,P5). So the pipe is below or almost below most of the sensors. This allows to observe the effect of group detachment on the pipe pressure response. During the video, the tip progressed by 18 mm. Figure 4 shows a screenshot of the video, including pipe contours (drawn manually).

Figure 3 shows the pipe pressure of, and the gradient between, different sensors at that time (4900<t<5100) together with an indication of the time of group detachment (D). The time of group detachment is observed from the video. At the start of the video (S), the pipe tip is stable. After the increase in head difference of 2 mm (H), the gradient upstream of the tip between P8 and P9 ($i_{8,9}$) increases to its maximum value, and then decreases towards the pipe gradient as the tip propagates upstream (and now $i_{9,10}$ increases). However, it can be seen that the decrease in $i_{8,9}$ is not gradual, but temporarily drops by approximately 0.02-0.03 after the first group detachment. The effect of the first group detachment on the pressures is also seen in the downstream gradient $i_{7,8}$ (temporary gradient increase) and to a lesser extent in $i_{6,7}$ (temporary gradient increases several seconds later). Similar pressure fluctuations were observed in tests on FPH and FS35 sand, but these could not be related to group detachment because of lacking close-up videos. Note that the head drop in P2 around t=4975 s is caused by local erosion of the pipe wall and not directly by group detachment. The fluctuations in gradient are larger than the

measurement uncertainty in pipe gradient (approx. 0.01), and its downstream propagation confirms that it is no sensor noise.

These effects of group detachment on the tip gradient seem small, but are approximately as large as the increase needed to start the erosion. This means that the tip gradient temporarily drops below the critical tip gradient and temporarily stops the tip erosion. These observations indicate that the transport of particles from the pipe tip affects the progression rate.

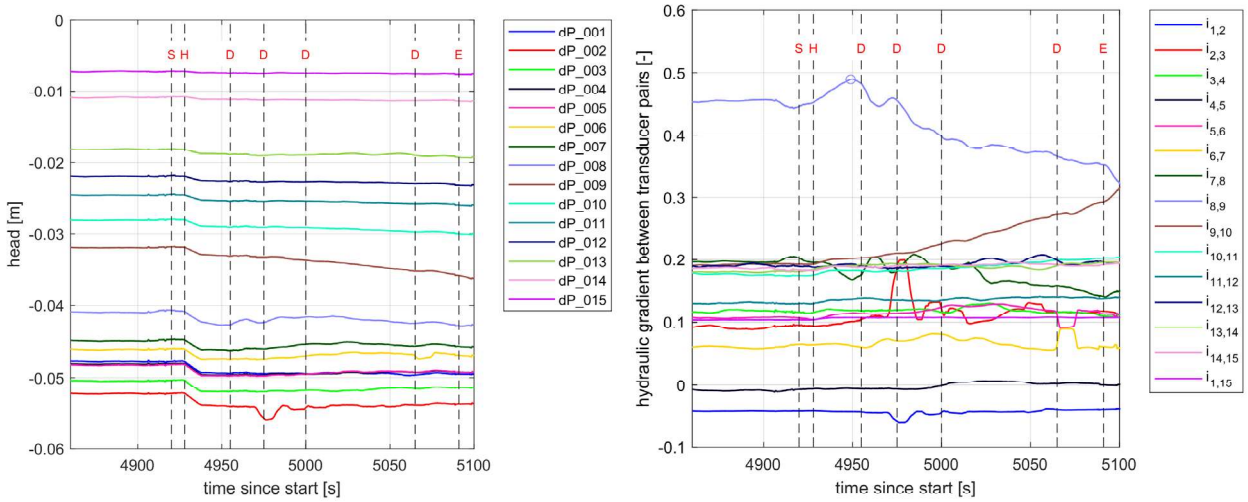

Figure 3. Pipe pressures (left) and gradients (right) during head increase and grain detachment. In red: S=start video, H=head increase, D=group detachment, E=end video. Right figure subscripts refer to the same "dP" sensors, downstream to upstream, on the left

Figure 4. Zone around pipe tip in test B25_245 s just before (t=4975s) and during (t=4976s) second group detachment.

Drivers of the progression rate

Kézdi (1979) proposed that the progression rate v is proportional to the seepage velocity just upstream of the pipe tip:

$$v = c\frac{ki_{s,tip}}{n}$$

in which k is the hydraulic conductivity, $i_{s,tip}$ the local hydraulic gradient just upstream of the pipe tip and c a coefficient. While Kézdi assumed that $i_{s,tip}$ equals the average gradient upstream of the tip, and no head loss in the pipe, this section applies the same concept using measured local tip gradients. The observations in the previous section suggest some influence of the particle transport in the pipe. If the progression rate depends on the sediment transport in the pipe, it may be related to the bed shear stress ($\tau_{bed,tip}$) just downstream of the pipe tip:

$$\tau_{bed,tip} = \rho_w g(a_{tip}/2)i_{p,tip}$$

in which ρ_w is water density, a_{tip} is pipe depth just downstream of the tip, and $i_{p,tip}$ is the gradient in the pipe just downstream of the tip. Here we assume $a_{tip}=1 \cdot d_{50}$ based on Vandenboer et al. (2019a) because we have no depth measurements (laser) during progression. This assumption is supported by our equilibrium depth measurements, which are not much deeper.

This section shows the relation between progression rate and both predictors: seepage velocity and bed shear stress. For each test, we selected the pressure ports where the tip passed right under. The tip gradients $i_{s,tip}$ corresponding to a certain pressure port equals the gradient between that pressure port and one port upstream at the time of passing. The pipe gradient $i_{p,tip}$ is the gradient between that pressure port and one port downstream, and is only included when the pipe passed under both pressure ports. Finally, the corresponding progression rate is calculated using a moving average (over 3 data points; usually 3 minutes) of the visually observed tip position. Since not all ports are passed, the number of data points varies between tests, and the number of data points with pipe gradient is smaller than the tip gradients.

Figure 5 shows that the progression rate is proportional to the seepage velocity for tests with normal loading (L1) on different sand types. However, the overloading tests (L3 and L4) on B25 sand show higher progression rates which cannot be explained by the seepage velocity. The right panel in Figure 5 shows that the bed shear stress is a slightly better predictor. Compared to the seepage velocity it also predicts the overloading tests reasonably well and explains part of the variation within groups (e.g. group *FS35,L1*).

The significant amount of scatter within tests may be the result of spatial variability in the sample, meandering, and measurement uncertainties. Effects of spatial variability and meandering cannot be quantified within the scope of this paper. Measurement uncertainties due to sensor error are estimated at 2% for tip gradients and 6% for pipe gradients. Pipes passing sensors at a small distance, may in a few cases have caused 10% underestimation of tip gradients and 10-50% error in pipe gradients. The smaller uncertainties in tip gradients (and seepage velocity) compared to pipe gradients (and bed shear stress) support the conclusion that the shear stress is a better predictor of the progression rate. Other uncertainties in the seepage velocity are that k and n equal the values of the undisturbed sample. Other uncertainties in the shear stress are

that the pipe depth was based on literature instead of measurements, the flow may not be steady, the pipe roughness may increase the friction, and the shear stress in the entire pipe may be relevant.

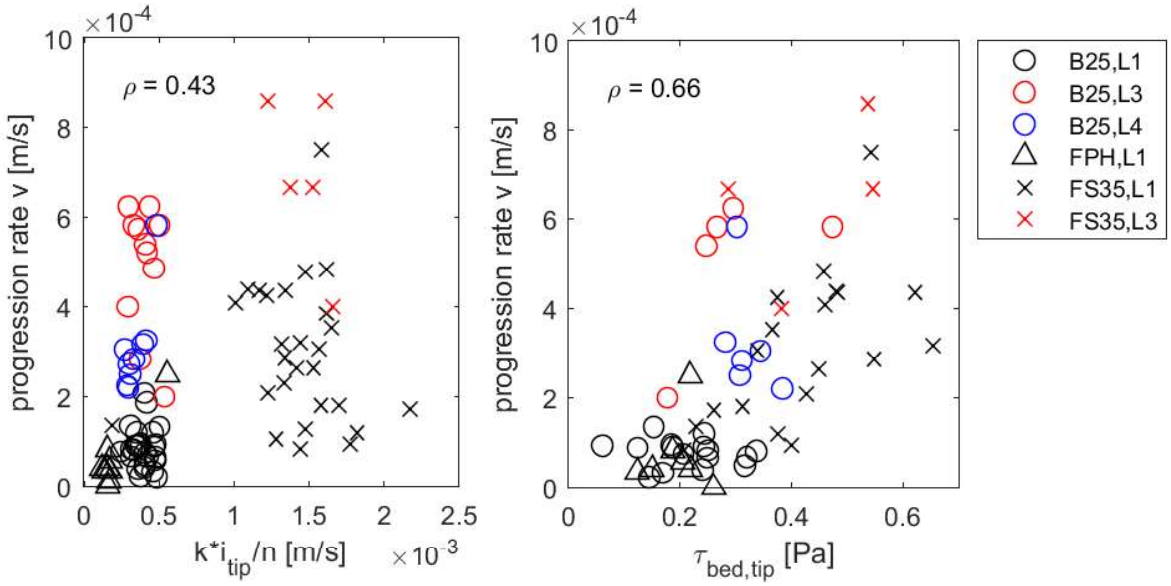

Figure 5. Relation between progression rate and seepage velocity (left) and bed shear stress (right). Color indicates loading type; marker indicates sand type. ρ=correlation coefficient.

CONCLUSIONS

This paper studies the parameters influencing the development of backward erosion piping over time. We conducted small-scale experiments with varying grain size, compaction, and hydraulic loading. We forced the pipe to grow under a row of pressure transducers to obtain pressure data with a high spatial and temporal resolution. This adapted setup yields measurements of the local hydraulic gradients throughout the pipe and in the region upstream of the pipe tip.

Analysis of high-resolution video and pipe pressure measurements in one test during a transition from equilibrium to erosion shows that the detachment of a group of particles leads to a temporary increase in pipe resistance. This results in a temporary drop of the local tip gradient, and a pause in the tip erosion. This indicates that the transport of particles from the pipe tip affects the progression rate.

Progression rates were correlated with seepage velocities just upstream of the pipe tip and bed shear stress just downstream of the pipe tip. The tests with gradual loading (pipe close to equilibrium) show a positive relation with seepage velocity (cf. Kézdi 1979; Robbins et al. 2017), but it cannot explain the higher progression rates in the test with overloading (higher than critical head). Bed shear stress correlates better with progression rate, including the overloading tests, and it also explains part of the variation in progression rate within tests on certain sand types.

Based on these findings, an improved model of pipe progression in dikes would include pipe shear stresses; directly through the correlations from Figure 5 or more detailed by modelling

sediment transport in combination with a local critical tip gradient. Non-steady numerical modelling of pipe progression in dikes has the potential to yield more accurate safety assessments and provide time-to-failure estimates during emergencies. As it requires the same input data as steady modelling, such a model would be quickly applicable to real dikes.

To improve the predictive value of the relation between progression rate and bed shear stress, it is recommended to perform additional tests with a wider range of grain sizes (0.1-1 mm) as well as longer seepage lengths and more severe overloading. Regarding the setup, it would be valuable to measure pipe depth continuously during pipe progression and to further reduce the pipe meandering.

REFERENCES

Allan, R.J. (2018). *Backward Erosion Piping.* PhD Thesis, UNSW Australia.

Bligh, W. (1910). "Dams, barrages and weirs on porous foundations." *Engineering News*, 64(26), 708-710.

Danka, J. and Zhang, L. (2015). "Dike failure mechanisms and breaching parameters." *Journal of Geotechnical and Geoenvironmental Engineering*, 141(9): 04015039.

Hanses, U. (1985). *Zur Mechanik der Entwicklung von Erosionskanalen in geschichtetem Untergrund unter Stauanlagen.* Universitatsbibliothek der TU Berlin, Berlin, Germany.

Kézdi, R. (1979). *Soil physics: selected topics*. Elsevier, Amsterdam, The Netherlands.

Miesel, D. (1977). "Untersuchungen zum Problem der rückschreitenden Erosion als Ursache des hydraulischen Grundbruches in Böden mit inhomogener Schichtfolge." In: *Veröffentlichungen des Grundbauinstitutes der Technischen Universität Berlin*, Berlin, 56-71.

Pol, J.C., van Beek, V.M., Kanning, W. and Jonkman, S.N. (2019). "Progression rate of backward erosion piping in laboratory experiments and reliability analysis." *7th International Symposium on Geotechnical Safety and Risk (ISGSR2019)*, J. Ching, D. Li, and J. Zhang, eds. Research Publishing, Singapore, 764–769

Robbins, B.A., Van Beek, V.M., Lopez-Soto, J.F., Montalvo-Bartolomei, A.M., & Murphy, J. (2017). "A novel laboratory test for backward erosion piping." *International Journal of Physical Modelling in Geotechnics*, 18(5), 266-279

Sellmeijer, J. (1988). *On the mechanism of piping under impervious structures*. PhD thesis, Delft University of Technology

Van Beek, V.M. (2015). *Backward erosion piping: Initiation and progression*. PhD thesis, Delft University of Technology

Vandenboer, K., van Beek, V. M., & Bezuijen, A. (2019a). "Analysis of the pipe depth development in small-scale backward erosion piping experiments". *Acta Geotechnica*, 14(2), 477-486

Vandenboer, K., Celette, F., & Bezuijen, A. (2019b). "The effect of sudden critical and supercritical hydraulic loads on backward erosion piping: small-scale experiments." *Acta Geotechnica*, 14(3), 783-794